Exp. Theo. NANOTECHNOLOGY 4 (2020) 59– 70 https://doi.org/10.56053/4.3.70

Synthesis and characterization of ZnO nanoflowers under temperature effect

W. Smith[1], *A. Becker*[2], *L. Harison*[1,*]

[1]Micro Materials Ltd, Ellice Way, Wrexham LL13 7YL, UK
[2]Department of Materials Science, Universidad Politécnica de Madrid, 28040 Madrid, Spain
*) Email: lharis@micromaterials.co.uk

Received 18/2/2020, *Accepted* 4/6/2020, *Published* 15/9/2020

Synthesis of flower-shaped ZnO nanostructures composed of hexagonal ZnO nanorods was achieved by the solution process using zinc acetate dihydrate and sodium hydroxide at very low temperature of 90 8C in 30 min. The individual nanorods are of hexagonal shape with sharp tip, and base diameter of about 300–350 nm. Detailed structural characterizations demonstrate that the synthesized products are single crystalline with the wurtzite hexagonal phase, grown along the [0 0 0 1] direction. The IR spectrum shows the standard peak of zinc oxide at 523 cm^{-1}. Raman scattering exhibits a sharp and strong E_2 mode at 437 cm^{-1} which further confirms the good crystallinity and wurtzite hexagonal phase of the grown nanostructures. The photoelectron spectroscopic measurement shows the presence of Zn, O, C, zinc acetate and Na. The binding energy ca. 1021.2 eV (Zn $2p_{3/2}$) and 1044.3 eV (Zn $2p_{1/2}$), are found very close to the standard bulk ZnO binding energy values. The O 1s peak is found centered at 531.4 eV with a shoulder at 529.8 eV. Room-temperature photoluminescence (PL) demonstrate a strong and dominated peak at 381 nm with a suppressed and broad green emission at 515 nm, suggests that the flower-shaped ZnO nanostructures have good optical properties with very less structural defects.

Keywords: Synthesis; Characterization; ZnO.

1. INTRODUCTION

Controlled synthesis of semiconductor nanostructures in terms of size and shape has been strongly motivated as the properties can be tailored by shape and size and novel applications can be investigated dependent on their structural properties [1–4]. Among various semiconductor nanostructures, variety of nanostructures of ZnO has been investigated presenting it as a richest family of nanostructures [5]. With a wurtzite hexagonal phase, ZnO have a direct band gap of 3.37 eV with the larger exciton binding energy (60 meV), possesses a wide range of technological applications including transparent conducting electrodes of solar cells, flat panel displays, surface acoustic devices, UV lasers and chemical and biological sensors [6–10]. Various methods such as thermal evaporation [11], hydrothermal process [12], cyclic feeding chemical vapor deposition [13], chemical vapor deposition (CVD) [14], metal–organic CVD [15], etc. have been applied to grow nanostructures of ZnO. In addition to these, solution method can produce such structures, without using metal catalyst or templates, with better crystal quality preferably at lower growth temperature; as well it works out to be an easier and economical process.

Zhang et al. reported synthesis of flower-shaped, snowflakes, prism, prickly spheres and rod-like morphologies using $Zn(OH)_4^{2-}$ or $Zn(NH_3)_4^{2-}$ as a precursor solutions (prepared in various solvents such as *n*-heptane, ethanol, water, etc.) at 180 8C for 13 h in a Teflon-lined autoclave [16]. Gao et al. reported the formation of flower-like ZnO nanostructures on silicon substrate at 95 8C in 60 min, by the thermolysis of ehthylenediamine–zinc complex with the assistance of hexamethylenetetramine in a laboratory Pyrex glass bottle with polypropylene autoclavable screw caps with the filling ratio of 80% [17]. Umetsu et al. reported the synthesis of ZnO nanostructures with the assistance of artificial peptides, at room temperature. They researched that the peptides can assist in the homogeneous assembly of ZnO nanoparticles into unique flower-like morphologies [18]. Hochepied et al. also synthesized the flower-shaped pompom-like particles from temperature-driven ammonia decomplexation at 85 8C in a 1 l water-jacked thermostated reactor, stirred mechanically by a four-blade propeller at 500 rpm [19]. Yang et al. presented the synthesis of flower- shaped, disk and dumbbell-like ZnO structures by the assistance of capping molecules such as citric acid and poly vinyl alcohol. These structures were grown into Teflon-lined stainless-steel autoclaves at 200 8C in 20 h [20]. In all the results reported above, the nanostructures were either grown using capping molecules and/or additives at higher temperatures (95–200 8C) requiring higher growth time. In this paper we described the synthesis of flower-shaped ZnO nanostructures via solution process using the zinc acetate dihydrate and NaOH only as a source material at 90 8C for 30 min. We found this method to be a simple, cost effective, and convenient route to obtain larger quantity of nanostructured zinc oxide. The synthesized products were elucidated in terms of their structural, chemical and optical properties.

2. EXPERIMENTAL DETAILS

Synthesis was carried out by solution process at 90 8C using zinc acetate dihydrate and sodium hydroxide (NaOH), as source materials. All the chemicals were purchased from Aldrich Chemical Corporation and used without further purification. For synthesis, 6.57 g zinc acetate dihydrate ($ZnAc_2$ $2H_2O$) was dissolved in 100 ml of de-ionized water under stirring at room temperature. Simultaneously, 3 M sodium hydroxide solution was added drop wise while stirring it continuously, resulting in a white milky precipitate. Before refluxing the solution, pH was measured as 13.2 by the expandable ion analyzer (EA 940, Orian). The solution was then transferred in a three-necked refluxing pot and refluxed at 90 8C for 30 min. The refluxing temperature was measured and controlled by k-type thermocouple and a PID temperature controller. While refluxing, the pH of the solution was not measured or controlled. After refluxing, the white powder was washed with methanol several times, dried at room temperature and was examined in terms of their structural, chemical and optical properties.

General morphologies and detailed structural characterizations were obtained using field emission scanning electron microscopy (FESEM). For SEM observation, the powder was uniformly sprayed on carbon tape. In order to avoid charging while observation, the powder was coated with thin platinum layer (10 nm). For the transmission electron microscopic measurement, powder was sonicated in ethanol for 10 min there by dipping copper grid in the solution and drying at room temperature. The crystallinity and crystal phases were determined by X-ray powder diffractometer (XRD) with Cu Kα radiation (1.54178 Å) with Bragg angle ranging from 208 to 658. The quality and composition of the synthesized flower-shaped ZnO nanostructures were characterized by the Fourier transform

infrared (FTIR) spectroscopy in the range of 400–4000 cm^{-1}. The surface states were analyzed by X-ray photoelectron spectroscopy (XPS, AXIS-NOVA, Kratos Inc.). Optical properties were analyzed by the UV–vis, Raman scattering and room temperature photoluminescence measurements.

3. RESULTS AND DISCUSSIONS

3.1 Detailed structural characterization of the flower-shaped ZnO nanostructures

Fig. 1 shows the general scanning electron morphologies of the synthesized structures. Fig. 1(a) and (b) shows the low magnification FESEM images whereas Fig. 1(c) and (d) presents the high magnification images of the grown

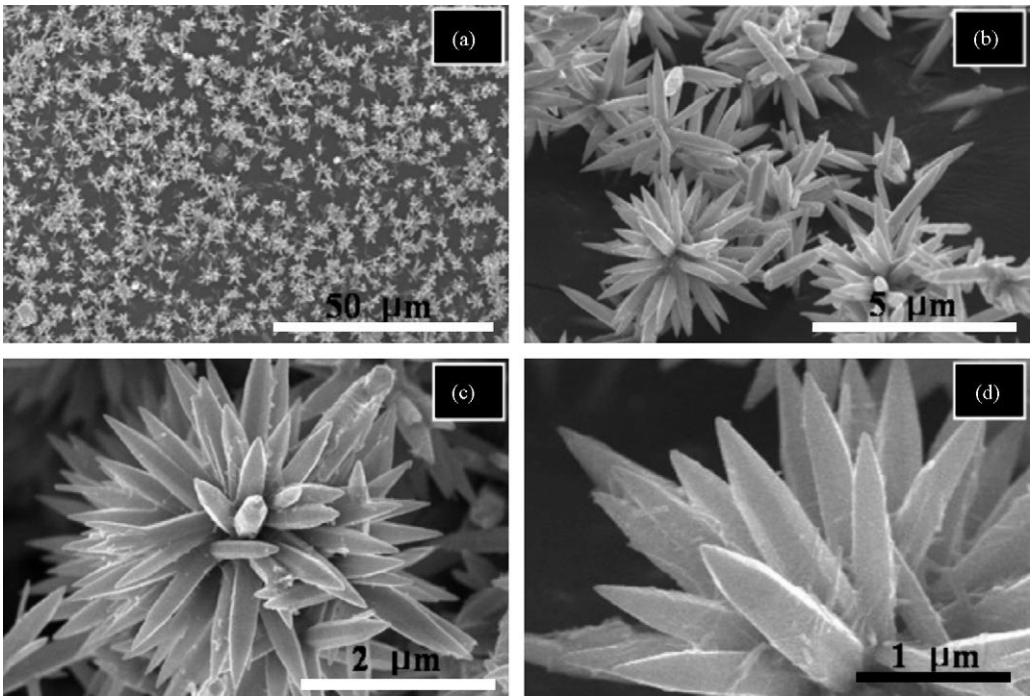

Figure 1 (a and b) Low and (c and d) high magnification FESEM images of flower-shaped ZnO nanostructures seen composed of hexagonal ZnO nanorods.

products. The images clearly reveal the flower-shaped structures that are composed of hexagonal nanorods. Magnified image shows that flower-shaped structures are constituted by the accumulation of several hundreds of sharp-tipped hexagonal ZnO nanorods. The typical diameters of these individual nanorods are in the range of 300–350 nm with the length of 2–4 *m*m. All the nanorods are seen originated from a single centre arranging them in a spherical shape exhibiting flower-like morphologies. The rod tip appears sharp with wide hexagonal-bases (Fig. 1(d)). The size of full array of a flower-shaped structure is in the range of 5–6 *m*m.

Fig. 2 presents the X-ray diffraction pattern of synthesized powder. All of the indexed peaks in the obtained spectrum are well matched with that of bulk ZnO (JCPDS Card No. 36–1451) which confirms that the synthesized powder is single crystalline and possesses a wurtzite hexagonal structure. No other peak related to impurities was

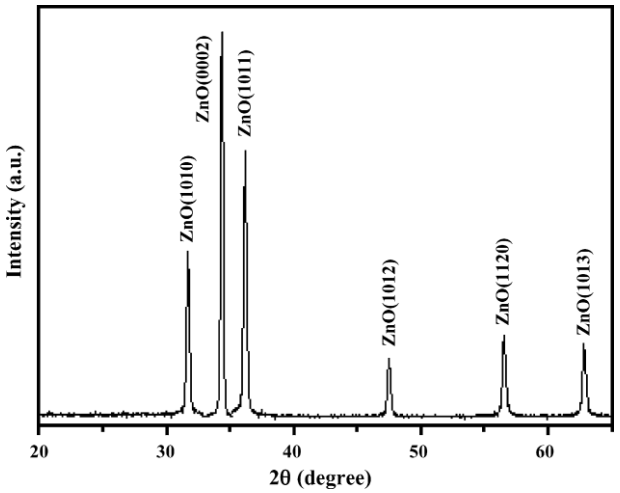

Figure 2 Typical X-ray diffraction (XRD) pattern synthesized nanostructure: the indexed peaks correspond to the wurtzite hexagonal phase.

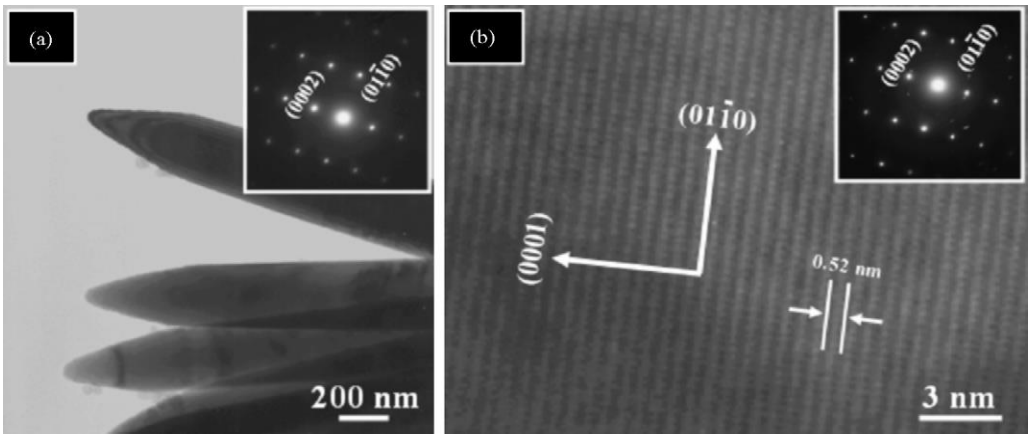

Figure 3 (a) Low magnification TEM image of the grown ZnO nanorods with their corresponding SAED pattern (inset). (b) HRTEM image showing the difference between two lattice fringes, which is about 0.52 nm. Corresponding SAED pattern (inset) is consistent with the HRTEM observation.

detected in the spectrum within the detection limit of the X-ray diffraction, which further confirms that the synthesized powders are pure ZnO. Additionally, higher intensity and narrower spectral width of ZnO (0 0 0 2) peak, compared to other observed ZnO peaks in the spectrum affirms the growth in *c*-axis direction.

Further structural characterization was carried out by the transmission electron microscopy (TEM) equipped with the selected area electron diffraction (SAED) setup. Fig. 3(a) shows the low magnification TEM image of the ZnO nanorods grown in the flower-shaped structures. The sharp tips and wider bases are clearly evident from this image. The base diameters are in the range of 300–350 nm. The corresponding SAED pattern obtained from the shown nanorods confirmed that the synthesized products are single crystalline and grew along the [0 0 0 1] direction (shown as inset in Fig. 3(a)). Fig. 3(b) shows the high-resolution TEM (HRTEM) image of a nanorod. The lattice fringes between two adjacent planes is about 0.52 nm which is equal to the lattice constant of the ZnO which further indicate that the obtained structure have a wurtzite hexagonal phase and are preferentially grown along the *c*-axis [0 0 0 1] direction. The corresponding SAED pattern (inset in Fig. 3(b)) is consistent with the HRTEM observation.

The composition and quality of the product was analyzed by the FTIR spectroscopy. Fig. 4 shows the FTIR spectrum which was acquired in the range of 400–4000cm^{-1}. The band at 523 cm^{-1} is correlated to zinc oxide [21]. The bands at 3200–3600 cm^{-1} correspond to O–H mode of vibration and the stretching mode of vibration of C O is observed at 1431 and 1652 cm^{-1}. Fig. 5 shows the room temperature UV–vis absorption spectrum of the synthesized powder. A broad band was observed in the spectrum at 373 cm^{-1} which is a characteristic band for the wurtzite hexagonal pure ZnO. No other peak was observed in the spectrum confirms that the synthesized products are ZnO only [22].

The sample was also characterized by X-ray photoelectron spectroscopy (XPS) in order to understand chemical bonding state of element; the corresponding spectra are presented as Fig. 6. The peak positions were referenced to carbon at 284.6 eV. Fig. 6(a) shows the wide scan spectrum of the sample, where peaks of Zn, O, C, zinc acetate and Na were detected. The presence of C can be due to the atmospheric contamination and ambient exposure of the sample, whereas Na peak is due to the sodium hydroxide used while synthesis. The presence of zinc acetate peak indicates that the acetate compound remained on the surface, probably due to low temperature synthesis. We expect that annealing of the powder will remove acetate. Fig. 6(b) and (c) shows the narrow scan spectra for Zn 2p and O 1s regions, respectively. The doublet spectral lines of Zn 2p are observed at the binding energy of 1021.2 eV (Zn $2p_{3/2}$) and 1044.3 eV (Zn $2p_{1/2}$), which are very close to the standard bulk ZnO binding energy values [23]. The O 1s peak is found centered at 531.4 eV with a shoulder at 529.8 eV. The core level O 1s spectrum, fitted with Gaussian–Lorentz distribution (70:30 ratio) with Shirley type base line is shown in Fig. 6(c). The O 1s peak is found built-up of sub-peaks at 529.25, 531.2 and 532.2 eV. The peak with low binding energy (529.25 eV) corresponds to the O–H surface adsorbed group. The peak centered at 532.2 eV is attributed to O^{2-} in the oxygen vacancies on the ZnO structure, whereas the peak at 531.2 eV is correlated to ZnO [24].

The expected growth process of the flower-shaped ZnO nanostructures composed of hexagonal nanorods can be explained by the initial precipitation of the $Zn(OH)_2$. The formed $Zn(OH)_2$ dissolves to a considerable extent in water

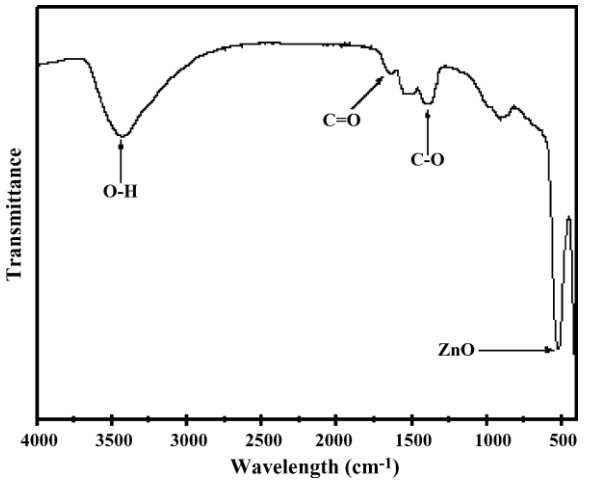

Figure 4 Typical FTIR spectrum of the synthesized nanostructure.

to form the Zn^{2+} and OH^- ions. Therefore, as the concentration of these Zn^{2+} and OH^- ions exceeds the critical value, the precipitation of ZnO nuclei starts. The transformation of the $Zn(OH)_2$ precipitates into the ZnO crystals proceed through these simple reactions:

The $Zn(OH)_2$ precipitates are more soluble as compared to the ZnO precipitates, hence the formed $Zn(OH)_2$ precipitate tends to produce continuously Zn^{2+} and OH^- ions which form the ZnO nuclei (I). The formed ZnO nuclei are expected to be the building blocks for the formation of the final products (II). Therefore, the ZnO nuclei concentration increases arranging themselves in a flower-shaped structure, due to surface energy.
The hexagonal nanorods with six defined facets arose to maintain the minimum surface energy as to keep the symmetry of the crystal structure (wurtzite ZnO). It is well known that the radii of newly formed crystal increase linearly with time after nuclei formation. As the new crystals grow, phase boundaries also increase at a given speed and eventually touch each other, forming the base of structure. Once base is formed, growth rate starts to decrease along the transverse direction and growth in the radial direction continues being the top surface an energetically favored surface.

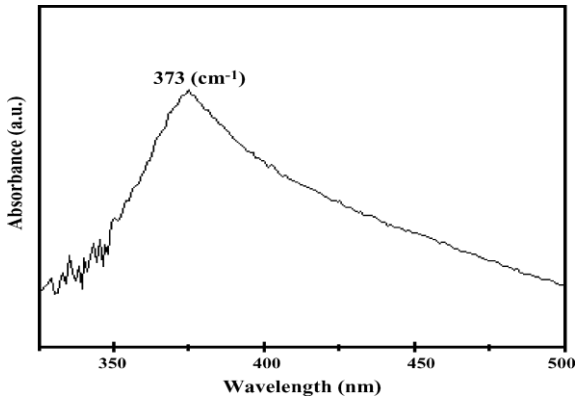

Fig. 5. Typical UV–vis spectrum of the synthesized nanostructure.

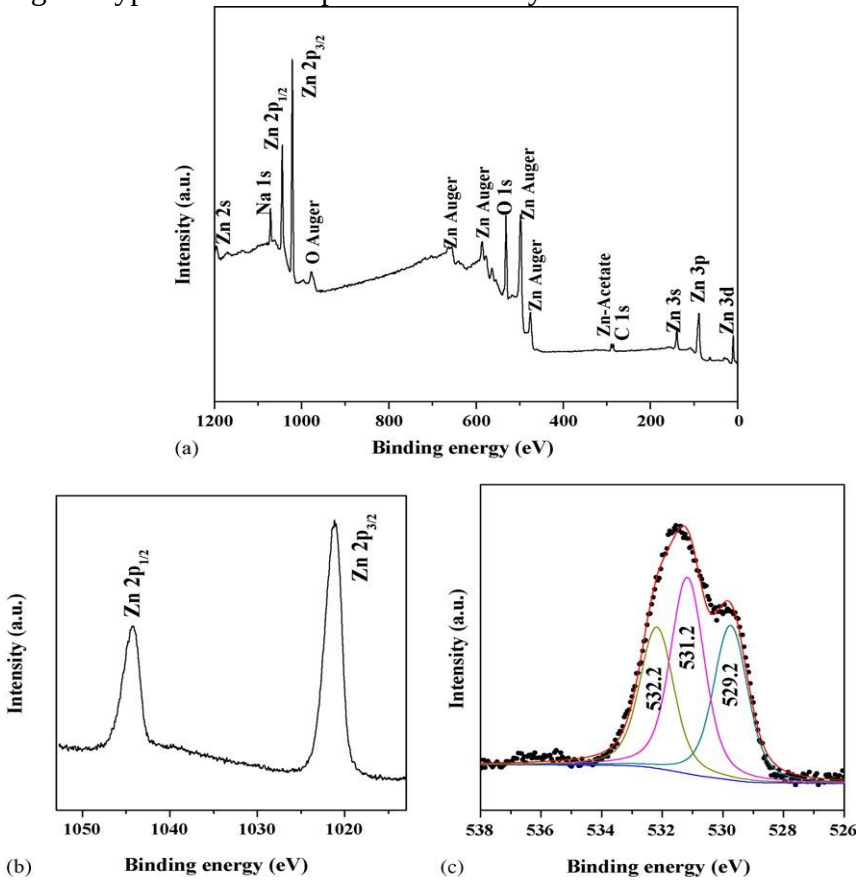

Figure 6 Photoelectron spectra of the synthesized powder: (a) wide scan survey, (b) core level spectrum for Zn 2p region and (c) core level O 1s spectrum, fitted with Gaussian–Lorentz distribution (70:30 ratio) with Shirley type base line.

Additionally as the ZnO is a polar crystal, where zinc and oxygen atoms are arranged alternatively along the *c*-axis and the top surfaces is Zn-terminated (0 0 0 1) while the bottom surfaces are oxygen-terminated $(0\,0\,0\,\bar{1})$. The Zn- (0 0 0 1) is catalytically active while the O- $(0\,0\,0\,\bar{1})$ is inert [25]. Therefore, the top surface would be energetically active. This will then help in growing in the radial direction once the nuclei are formed. The formation of tip at the edge is correlated to the different growth

velocities in different growth planes, as explained below.
The growths are also dependent upon the growth velocities of different growth planes in the ZnO crystals. Laudise and Ballman reported that the higher the growth rate, the quicker the disappearance of plane, which leads to the
pointed shape in end of the *c*-axis [26]. In ZnO, the growth velocities of the ZnO crystals in different directions are $[0\,0\,0\,1] > 0\,1\,\bar{1}\,\bar{1} > 0\,1\,\bar{1}\,0 > 0\,1\,\bar{1}\,1 > 0\,0\,0\,\bar{1}$, under hydrothermal conditions [27]. Therefore, the (0 0 0 1) plane, the most rapid growth rate plane, disappears which leads to the pointed shape in an end of the (0 0 0 1) plane. Moreover, the $0\,0\,0\,\bar{1}$ plane has the slowest growth rate which leads to the plain shape in another end. In our synthesized nanostructures, all the observed nanorods have pointed tips with the flat down surfaces which is consistent with the growth habit of ZnO crystals.

3.2 Optical properties of the flower-shaped ZnO nanostructures

The optical properties of the synthesized flower-shaped ZnO nanostructures were observed by the Raman scattering and room-temperature photoluminescence measurements. The Raman spectra are sensitive to the crystal quality,

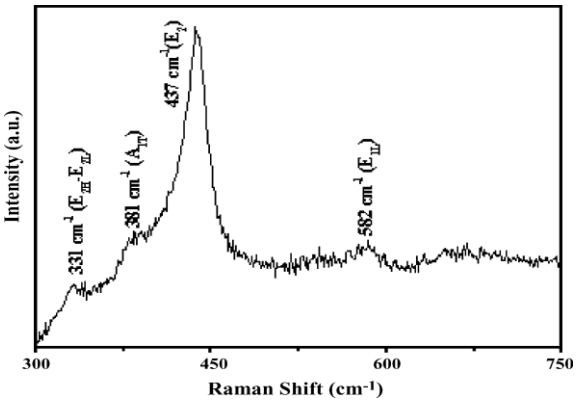

Figure 7 Typical Raman spectrum of the synthesized nanostructure.

structural defects and disorders of the grown products. With a wurtzite hexagonal, ZnO with two belongs to the C^4

formula units per primitive cell. The primitive cell includes two formula units in which all the atoms are occupying the 2b sites of the C_{3v} symmetry. Group theory predicts, at the G point of the Brillouin zone, there is an existence of following optic modes: $G = A_1 + 2B_1 + E_1 + 2E_2$. The A_1, E_1 and E_2 modes are Raman active. Furthermore, the A_1 and E_1 are infrared active and splits into longitudinal optical (LO) components and transverse optical (TO) components [28]. Fig. 7 shows the Raman spectrum of the synthesized powder. A sharp and strong peak at 437 cm^{-1} is observed which is attributed to the optical phonon E_2 mode of the ZnO and a characteristic Raman active peak for the wurtzite hexagonal phase of ZnO [29]. Furthermore, two very small peaks at 331 and 381 cm^{-1} are also observed in the spectrum which are assigned to be as E_{2H}–E_{2L} (multi phonon process) and A_{1T} modes, respectively. Additionally, a very suppressed and short peak at 582 cm^{-1} is seen in the spectrum and attributed as E_{1L} mode [30,31]. The origination of E_{1L} mode in the Raman scattering is because of the impurities and structural defects (oxygen vacancies and Zn interstitials) of the synthesized products. Therefore, the presence of high intensity E_2 mode with the suppressed and very short E_{1L} peak in the Raman scattering indicate that the synthesized flower-shaped ZnO nanostructures are good in crystal quality and possesses the wurtzite hexagonal crystal structure.

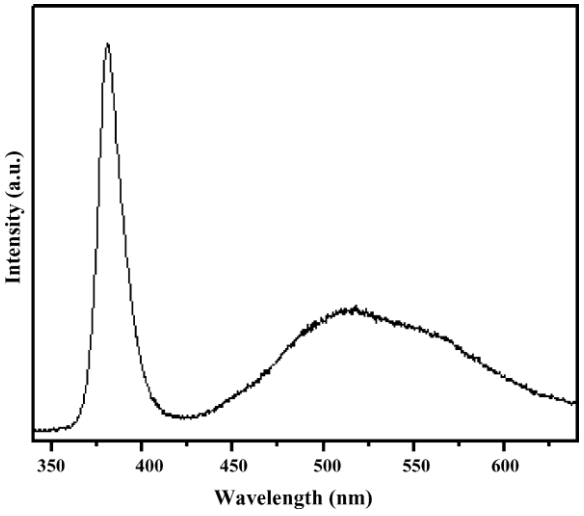

Figure 8 Room-temperature photoluminescence (PL) spectrum of the synthesized nanostructures acquired using a He–Cd laser-line with an excitation wavelength of 325 nm.

Fig. 8 shows the room-temperature photoluminescence spectrum of the synthesized powder. An intense, sharp and dominated peak at 380 nm in the UV region and a suppressed and broad band at 515 nm are observed. The UV emission, also called as near band edge emission, generated by the free-exciton recombination while the green emission, also known as deep level emission, appeared because of the impurities and structural defects in the deposited structures. The green emission is because of the recombination of electrons in single occupied oxygen vacancies in ZnO while the UV emission is because of the recombination of a photogenerated hole with an electron occupying the oxygen vacancies. Generally, high crystalline quality ZnO shows a

dominated UV emission with a week green emission. Bagnall et al. reported that the crystal quality of the deposited ZnO is important factor for the high UV emission and hence betterment in the crystal quality (less structural defects and impurities such as oxygen vacancies and zinc interstitials) may enhance the intensity of UV emission [32]. In our case, the near band edge emission is dominated over the deep level emission, which indicates that the grown nanostructures are good in crystal quality and exhibiting a good optical property.

4. CONCLUSIONS

Synthesis of flower-shaped ZnO nanostructures composed of hexagonal ZnO nanorods was achieved by the solution process using zinc acetate dihydrate and sodium hydroxide at low temperature, i.e. 90 8C in 30 min. Detailed structural characterizations demonstrate that the synthesized products are single crystalline with the wurtzite hexagonal phase, grown in the *c*-axis direction. The sharp tips and wider bases are clearly evident from SEM/TEM images. The base diameters are in the range of 300–350 nm. A photoelectron spectroscopic measurement shows the presence of Zn, O, C, zinc acetate and Na. The doublet spectral lines of Zn 2p are observed at the binding energy of 1021.2 eV (Zn $2p_{3/2}$) and 1044.3 eV (Zn $2p_{1/2}$), which are very close to the standard bulk ZnO binding energy values. The O 1s peak is found centered at 531.4 eV with a shoulder at 529.8 eV. The UV–vis, Raman scattering and room- temperature photoluminescence measurements indicate that the synthesized products are single crystalline ZnO exhibiting a good optical property.

References

[1] Arafa H. Aly, Ahmed Mehaney, Shrouk Eid, Exp. Theo. NANOTECHNOLOGY 3 (2019) 19

[2] W.J.E. Beek, M.M. Wienk, R.A.J. Janssen, Adv. Mater. 16 (2004) 1009

[3] W.J.E. Beek, M.M. Wienk, M.K. Emerink, X. Yang, R.A.J. Janssen, J. Phys. Chem. B 109 (2005) 9505

[4] Y. Xia, P. Yang, Y. Sun, Y. Wu, B. Mare, B. Gates, Y. Yin, F. Kim, H.Yan, Adv. Mater. 15 (2003) 323

[5] Z.L. Wang, Mater. Today 7 (2004) 26

[6] P. Zu, Z.K. Tang, G.K. Wong, M. Kawasaki, A. Ohtomo, H. Koinuma, Y. Segawa, Solid State Commun. 103 (1997) 459

[7] D.M. Bangall, Y.G. Chen, Z. Zhu, T. Yao, Appl. Phys. Lett. 70 (1997) 2230

[8] Y.C. Kong, D.P. Yu, B. Zhang, W. Fang, S.Q. Feng, Appl. Phys. Lett. 78 (2001) 407

[9] Y. Li, G.W. Meng, L.D. Zhang, F. Philip, Appl. Phys. Lett. 76 (2000) 2011

[10] K. Omichi, K. Kaiya, N. Takahashi, T. Nakamura, S. Okamoto, H. Yamamoto, J. Mater. Chem. 11 (2001) 262

[11] H. Huang, Y. Wu, H. Feick, N. Tran, E. Weber, P. Yang, Adv. Mater. 13 (2001) 113

[12] Y. Wang, M. Li, Mater. Lett. 60 (2006) 266
[13] A. Umar, S. Lee, Y.S. Lee, K.S. Nahm, Y.B. Hahn, J. Cryst. Growth 277 (2005) 479
[14] C.L. Wu, Li Chang, H.G. Chen, C.W. Lin, T.F. Chang, Y.C. Chao, J.K. Yan, Thin Solid Films 498 (2006) 137
[15] J.Y. Park, H. Oh, J.-J. Kim, S.S. Kim, J. Cryst. Growth 287 (2006) 145
[16] J. Zhang, et al. Chem. Mater. 12 (2002) 4172
[17] X. Gao, X. Li, W. Yu, J. Solid State Chem. 178 (2005) 1139
[18] M. Umetsu, M. Mizuta, K. Tsumoto, S. Ohra, S. Takami, H. Watanabe, I. Kumagaiand, T. Adschiri, Adv. Mater. 17 (2005) 2571
[19] J.F. Hochepied, A.P.A. Oliveira, V.G. Ferrol, J.F. Tranchant, J. Cryst. Growth 282 (2005) 156a
[20] H. Zhang, D. Yang, D. Li, X. Ma, S. Li, D. Que, Cryst. Growth Des. 5 (2005) 547
[21] W. Lili, W. Youshi, S. Yuanchang, W. Huiying, Rare Metals 25 (2006) 68
[22] Y.H. Ni, X.W. Wei, J.M. Hong, Y. Ye, Mater. Sci. Eng. B 121 (2005) 42
[23] B. Vincent Crist, Handbook of Monochromatic XPS Spectra: The Elements and Native Oxides, John Wiley & Sons, England, 2000, p. 510
[24] http://srdata.nist.gov/xps/bind_e_detail_indv.asp?ID1=22608
[25] P.X. Gao, Z.L. Wang, J. Phys. Chem. B 108 (2004) 7534
[26] R.A. Laudise, A.A. Ballman, J. Phys. Chem. 64 (1960) 688
[27] W.J. Li, E.W. Shi, M.Y. Tian, B.G. Wang, W.Z. Zhong, Sci. China E 28 (1998) 212
[28] T.C. Damen, S.P.S. Porto, B. Tell, Phys. Rev. 142 (1966) 142
[29] Y.J. Xing, Z.H. Xi, Z.Q. Xue, X.D. Zhang, J.H. Song, R.M. Wang, J. Xu, Y. Song, S.L. Zhang, D.P. Yu, Appl. Phys. Lett. 83 (2003) 1689
[30] M. Rajalakshmi, A.K. Arora, B.S. Bendre, S. Mahamuni, J. Appl. Phys. 87 (2000) 2445
[31] K. Vanheusden, C.H. Seager, W.L. Warren, D.R. Tallant, J.A. Voigt, J. Appl. Phys. 79 (1996) 7983
[32] D.M. Bagnall, Y.F. Chen, Z. Zhu, T. Yao, S. Koyama, M.Y. Shen, T. Goto, Appl. Phys. Lett. 73 (1998) 1038